MULTIPHASE FLOW IMAGING BY CAPACITANCE TOMOGRAPHY USING SIMULATED ANNEALING INVERSION

Roland Martin, Carlos Ortiz-Aleman and Carlos Gamio

Abstract. Electrical capacitance tomography (ECT) is a technique for obtaining cross-sectional images of the electrical permittivity distribution inside an electrically non-conducting body. It can be used to map the composition of two-phase mixtures like gas-oil systems and provides a useful tool for multiphase flow visualization and measurement and potential applications in petroleum industry. The ECT sensor collects the measured capacitances which are then inverted with a suitable reconstruction algorithm in order to produce an image of the permittivity distribution. But the linear, iterative or regularizing inversion techniques commonly used introduce unwanted smoothing effects in the reconstructed images, may become unstable or may not converge towards the desired solution.

In this work we apply the simulated annealing (SA) method to the reconstruction images from ECT measurements. The forward problem is calculated by using a finite volume space discretization mehod to avoid geometrical singularities (as occurs with a classical finite difference method), and to take advantage from its conservative formulation. We test the SA inversion method using static physical models and simulate the typical distribution patterns of two-component flows. This inversion technique has some advantages over approaches based on damping least-square inversions: they find good solutions starting with poor initial models, implement more easily complex a priori information, and do not introduce smoothing effects in the final permittivities.

Keywords: Simulated annealing, capacitance tomography, finite volumes

AMS classification: 86A22, 35R30, 68W10

§1. Introduction

In the last two decades, Electrical Capacitance Tomography (ECT) has been developed for non intrusive tomography purposes. This technique is used to obtain cross sectional images of the permittivity distribution into the inner core or region of a non conductive body [10]. By this mean, the composition of two-phase mixtures like gas-solid or gas-oil systems can be mapped by this mean and many potential applications in visualization and measurement of multiphase

flows for the oil industry have been performed to study oil-gas pipe flows, gas-solid distributions in pneumatic conveyors and fluidized beds, flame combustions, water hammers, water-oil-gas separation processes and trickle bed reactors for measuring water contents [11]. In this context, a ECT multisensor system is constituted by an insulating tube with a certain number of electrodes in its outer wall surrounded by an external screen. The use of cylindrical guards allows to model the multisensor as a two dimensional problem [9]. The sensor is connected to a device which measures mutual capacitances between every possible pair of electrodes. The data collected in this way are then inverted by an appropriate reconstruction algorithm and an image of the permittivity distribution is produced in the sensor. The inversion solver assumes the resolution of a forward problem for each electrode problem.

The first ECT system was developed by the US Department of energy to image gas-solid distributions in fluidized beds and gas-oil pipe flow imaging [7]. The first real time ECT system has been performed at UMIST at the beginning of the 1990s to visualize two-phase flow systems in pipelines [3, 10]. In those years and the following, different hardware process systems have been developed using four to sixteen electrodes in this context thanks to the improvement of the electronic transducers [4]. Since 1995, the needs of process applications have increased and made possible due to the significant improvement of the design and the operation of the process plants equipment [1]. The ECT technique has become the most powerful tool used to reconstruct images of turbulent multiphase flows. Until now, the most complex reconstructed flows have concerned two phase stratified flows issuing from wells, pneumatic conveyors and gas-solid fluidizations [7], and trickle bed reactors for measuring water content [11].

During these last twenty years, many imaging reconstruction algorithms have been used and are generally classified in iterative and non-iterative techniques [11]. Their main purpose was to improve the yet available image reconstruction methods. However, so far simple direct methods like linear back-projection (LBP) yield relatively poor images that only provide a qualitative indication of the component distribution inside the sensor. LBP is based on making a linear approximation to a problem that is essentially non-linear [6]. Therefore, this image reconstruction method causes considerable errors, which are particularly grave if there are large permittivity differences in the image. So far, the main alternative to LBP has been the use of iterative methods that seek to minimize some objective function, employing local optimization techniques like the regularized Newton-Raphson method or other similar approaches [11]. These methods are based on minimizing, with respect to the permittivity distribution, a L^2 functional involving the misfit function between computed and measured mutual capacitances, and a regularization matrix function containing some type of a-priori smoothness information about permittivities. Starting with an initial guess permittivity distribution, the minimization is carried out by an iterative procedure (basically a Newton-type method with Tikhonov regularization). The main problems of these iterative local optimization techniques are that they generally require one or more regularization parameters whose optimal value depends precisely on the (unknown) image to be reconstructed, and that they smooth the image contour. If the regularization is too strong the smoothing effects will appear, and it is too slight the technique. Thus, better and more accurate image reconstruction methods are still being developed in the context of this application.

In the last decades, an important improvement of geophysical data processing and modeling techniques related to inversion theory and global optimization has been done. The inverse problem starts from the data and an appropriate model in order to estimate the parameters of

the model. The inversion methods use the direct modeling in an iterative process. When the resolution of the direct problem is not too much time consuming, the problems can be treated very efficiently using techniques of global optimization. These techniques are really attractive because they can overwhelm many classical limitations of the local methods. The global optimization technique explore the whole set of solutions during the iterative process. In spite of the existence of partial solutions, the probability of a smaller and better misfit between synthetic and observed data is higher. These methods do not require the use of the objective function gradient because the problem do not need to be linearized. Global optimization algorithms need stochastic criteria to explore simultaneously the whole space of solutions and find the optimal model. The most famous global algorithm is the Monte Carlo method which performs the research randomly. At each new generated model, the information obtained from the previously evaluated models are not taken into account [2]. Among all the global optimization techniques, the genetic algorithms (GA) and the simulated annealing (SA) algorithms have proved to be efficient for many problems of interest in geophysics (exploration, magnetometry, gravimetry). Both have been conceived as optimization systems occurring in nature.

In this study we have chosen the SA algorithm in order to obtain an accurate image of complex flows. The convergence of SA is highly dependent of the resolution technique employed in the forward (or direct) problem. SA can be identified as a non-linear multi-parameter optimization method and a stochastic search technique. SA is also a generalization of Monte Carlo methods for examining the equations of state and frozen states of n-body systems [5]. A description of SA is given in the second section of this paper. The forward problem involved at each iteration of the SA algorithm uses here a finite volume method (FVM) formulated in polar coordinates in order to earn CPU time and be more accurate than methods using finite element and finite difference spatial schemes commonly introduced by many groups working in this field of interest. The most important topic we point at in this paper is the feasibility of such algorithms using a more suitable arrangement of permittivity distributions in the FVM mesh than the one used in [6]. The parameters of the inverse problem are chosen this way so as to converge faster. The mesh has an impact on the rate of convergence of the whole algorithm and the accuracy of the solution, and the Bi-Conjugate Gradient linear solver is fully coupled with the iterative process of the inverse problem in order to take in to account the solutions computed in previous iterations. In the forward problem, usually the Finite Element Method is used [10] and the commercial software OPERA seems to be the reference direct solver. It uses a three step decomposition of the matrix by diagonalization. Its main problem is that the whole system must be solved for each electrode combination problem. Here we propose a finite volume approach in a polar configuration and an accelerated BICG linear solver that allows us to decrease efficiently the time consuming of the linear system resolution.

§2. The Inversion Algorithm

2.1. The Forward Problem Solver

The forward problem is solved by using a finite volume method in a cylindrical configuration, in order to avoid undefined solutions at the disk centre and make the mesh refinement more flexible in comparison with finite element methods. We solve the following equations:

$$\nabla \cdot (\epsilon \nabla \phi^k) = 0 \tag{1}$$

where ϵ is a given permittivity distribution in the disk domain and ϕ^k is the potential field to be computed when the electrode k is the potential source. Dirichlet boundary conditions are applied on the source electrodes ($\phi^k = V$), and on the receiver electrodes and on the external screen ($\phi^k = 0$)

Defining the radius and angle coordinates as r and θ, and using the finite volume method, the discretized equation is formulated in the conservative form on each cell Ω_{ij}:

$$\int_{\Omega_{ij}} \nabla \cdot (\epsilon \nabla \phi^k) d\Omega_{ij} = 0 \tag{2}$$

for $i = 1, ..., N_r$ and $j = 1, ..., N_\theta$, where i and j are related to the spatial discretization along the directions r and θ respectively, and N_r and N_θ being the number of grid points in the radial and angular directions.

Applying the Gauss theorem, and using polar coordinates, the discretized equations can be written as:

$$\int_{\Gamma_{ij}} \epsilon \nabla \phi^k \cdot d\Gamma_{ij} = 0 \tag{3}$$

where Γ_{ij} is the boundary of the finite volume cell Ω_{ij}. The boundary is defined by Γ_W and Γ_E along the radial coordinates, and by Γ_N and Γ_S along the angular coordinates. Equation (3) can be expressed as the sum of the fluxes through the faces Γ_N, Γ_S, Γ_E and Γ_W :

$$\sum_l (\int_{\Gamma_l} \epsilon \nabla \phi^k \cdot n_l d\Gamma_l) = \sum_{i=S,N} (\epsilon \frac{\partial \phi}{\partial r} r \Delta\theta) \mid_i + \sum_{i=W,E} (\frac{\epsilon}{r} \frac{\partial \phi}{\partial \theta} \Delta r) \mid_i = 0 \tag{4}$$

From equation (4), the term corresponding to the fluxes at zero radius location vanishes and the problem is equivalent to solve the equations close to the center on triangles having a vertex at the center. Then, the discretized system of equations is well posed. The whole system is similar to a Laplacian equation system and a band diagonal linear system must be solved including the periodic boundary conditions imposed by the geometry of the problem. The corresponding matrix is positive definite and non symmetric. The mutual capacitances on each electrode are computed integrating the potential gradients along the electrode length according to the following expression:

$$C_{ij} = \frac{Q_i}{V_j} = -\frac{\epsilon_o}{V} \int_{\Gamma_i} (\epsilon \nabla \phi^j) \cdot d\mathbf{l} = -\frac{\epsilon_o}{V} \int_{\Gamma_i} \epsilon \frac{\partial \phi^j}{\partial n} dl \tag{5}$$

where n is the normal to the electrode contour, ϕ^j is the electrostatic potential created in the sensor by a voltage V to the electrode j, ϵ_o is the vacuum permittivity (8.854×10^{-12} Farads/m), Γ_i is a boundary enclosing the electrode i, $d\mathbf{l}$ is an infinitesimal element of the curve (in 2D) or surface (in 3D) Γ_i. The integration is performed using a trapezoidal rule and the potential gradients are computed to the fourth order.

To solve the twelve problems at each iteration of the inverse problem, commercial finite element based solvers like OPERA [10]which use a matrix diagonalization take close to ten seconds on a Pentium III computer to obtain all the 66 capacitances for a 3000 points grid. In our case, we reach 5s with BiCG technique. This is due to the fact that in OPERA the diagonal matrix, the upper triangular matrix and its transpose are stored before solving the twelve forward problems but the three step resolution must be done for each problem. The algorithm is of order $\theta(N^3)$ while the BiCG solver used here is of order $\theta(N^2)$ and can be easily

parallelized on a PC cluster supercomputer. In order to accelerate the bi-conjugate gradient linear solver, the twelve potentials computed at the previous iteration of the inversion problem are set as first guesses of the twelve new forward problems of the present new inverse problem iteration. The number of iterations per each forward problem is then quite random but always remains lower than the number of iterations at the first step of the whole inversion process.

The errors between measured and calculated data can be really high with variations as important as 20%. We have ponderated the computed capacitances by an amount error coming from well known measured and computed data in the case of an empty sensor (only air). In the empty sensor case, the errors between the FVM computed capacitances and the true data are shown in figure 1 using a logarithmic scale. The worst errors between computed and measured capacitances are related to the electrodes (here electrodes 1 and 11) adjacent to the source electrode (here the electrode 12). The non-adjacent capacitances are really better computed.

2.2. Parameter calibration in the mesh

For a given number of points in a polar mesh configuration, different radial and angular increments Δr and $\Delta\theta$ are possible. The angular steps are very sensible parameters that influence the calculation of the solution. We have then chosen a number of 240 equal angular steps. In order to compute more accurately the capacitances and to have less contrasts in the areas of the cells in the mesh, it is more convenient to refine the mesh from the center to the electrodes with the non-unique configuration shown in figure 2. In this figure, the mesh with a constant radius is oversampled near the center and the cells are too coarse to have a good solution near the electrodes while the non constant radius cells have less oversampling in the center and provide more accuracy close to the electrodes for a same number of points as in the other mesh. The inversion algorithm convergence is extremely dependent on the mesh construction and how the permittivity parameters to be inverted are arranged at the mesh points. For a given N_r by N_θ mesh and taking an analogue strategy than in multigrid techniques, each permittivity parameter is assigned to a block B_k of n_p volumes such that its area is equal to the area of the other blocks. Each volume is related to a point of the mesh located at the center of this volume. The other blocks can contain different number of volumes or mesh points. This arrangement allows an equal area weighting of the different permittivities to be inverted and equivalent impacts of the permittivity perturbations during the inversion process. For reasons of accuracy the number of permittivity parameters must be increased and so must be the number of blocks during the process. The number of blocks is refined in one direction and after many thousands iterations the number of blocks is increased in the other direction. This allows to refine uniformly the set of parameters in the mesh and to search other optima during the inversion process. The whole process is equivalent to model first coarse structures with coarse blocks in the mesh until a certain level accuracy of the capacitance misfit function is reached, then the finer structures with finer blocks are computed according to the finding of new optima and so on. At the end a uniform permittivity distribution related to the volume blocks is formed with a good accuracy turning around 10^{-6} for a L^2 norm choice of the misfit function. At the beginning of the process, it is not necessary to choose a too low tolerance error in the BiCG linear solver because the misfit is not good enough. Then we choose a 10^{-5} (not too low) starting error that we impose to decrease by roughly an order of magnitude each 10^4 iterations approximately during the inversion iterative process.

2.3. The Simulated Annealing Algorithm

The simulated annealing method is based on an analogy with the thermodynamic process of crystallization. A mineral fluid that cools slowly until it reaches a low energy state, gives rise to the formation of well defined crystals. If, on the contrary, the substance leaves its thermal equilibrium state with a sudden or partial cooling, the resulting crystal will have many defects, or the substance may even form a 'glass', characterized by its meta-stable molecular disorder. This concept is used in the context of optimization methods to recognize potentially useful models or configurations.

The atoms of each molecular configuration are equivalent to the model parameter in the inverse problem (i.e., the permittivity of the various image pixels). The system energy for such configuration is related to the cost (or misfit) function associated with the set of parameters involved in the model. In our case, the system energy is associated with the following L^2 norm:

$$E = \frac{\sum_{j=1,m}(c(j)_{obs} - c(j)_{calc})^2}{\sum_{j=1,m}(c(j)_{obs})^2} \tag{6}$$

where $c(j)_{obs}$ are the m measured capacitances and $c(j)_{calc}$ are the ones calculated by solving the forward problem for a given permittivity distribution ϵ. From an initial permittivity distribution, the method generates a range of configurations or parameter combinations considering a certain temperature T for the process. For this purpose the Metropolis criterion is employed, which consists in changing a parameter, in each iteration, by a small random amount. This shift causes a change E in the system's total energy. If ΔE is less than or equal to zero, the change in the parameter is accepted and the resulting configuration is considered as the new current configuration. When there is an increase in the system energy (E is greater than zero), the probability of acceptance or rejection for the parameter change is determined as

$$P(\Delta E) = e^{-\Delta E/T} \tag{7}$$

In order to decide whether or not a change that produces an increase in the system energy is accepted, a random number between zero and one is chosen, which is then compared with the value of the probability corresponding to E. If said random number is smaller, the parameter shift is accepted and the new configuration is considered as the current (updated) one. If said random number is greater, the parameter shift is not accepted and the configuration that existed before the shift is maintained. Repeating this procedure continuously, the thermal movement of the atoms of a system in thermal equilibrium (at a fixed temperature T) is simulated. In order to reach the system's base state, that is to say, the state of lowest energy and highest order, the temperature must be reduced very slowly, simulating a quasi-static process. This means that, during the cooling, the system must experience a series of states infinitesimally separated from the state of thermal equilibrium.

The method of simulated annealing has three basic components [8]: an energy (or cost, or misfit) function, an order function (the Metropolis criterion), and a parameter that controls the system temperature. The process consists of three nested cycles. Figure 3 shows a diagram that illustrates how the method works.

The external cycle (3) regulates the system temperature. Every time a cycle is completed, the temperature decreases as it is multiplied by a factor RT that is normally very close to one ($0 < RT < 1$). In this way the desired slow and gradual cooling is carried out. The intermediate

cycle (2) updates the values, independent of each other, of a series of constants K_i associated with each parameter. Said constants determine the maximum change that each parameter may experience when it is perturbed in the innermost cycle (1). The value of said constants depends on the number of times that the current model has been accepted (according to the Metropolis criterion) at the end of every sequence of internal cycles (1). In the internal cycle (1) the parameter values are perturbed using the factors K_i , defined in the intermediate cycle (2). The perturbation is done multiplying each parameter by the product of its corresponding K_i times a randomly chosen number between minus one and one. After this, the synthetic response of the current model is calculated and the change in the system's energy associated with the new parameter configuration is evaluated. Said energy change corresponds to the misfit between the synthetic data curve and the observed or measured one. If the misfit decreases, then the new configuration will be accepted as the current one and in turn perturbed in the same way. If, on the contrary, the random perturbation causes an increase in the misfit, associated with an increment in the energy E, then a probability of acceptance according to the Metropolis criterion is assigned to that configuration.

The cycles (1), (2) and (3) are repeated, while the temperature of the process decreases progressively. As the temperature diminishes, the parameter variations are smaller and smaller. In this way, the search in the solutions domain tends to confine itself towards the models associated with the absolute minimum of the misfit function E. The end result is a set of values for the parameters (i.e., the permittivity in the various pixels that make an image) whose synthetic response reproduces the observed (capacitance) data, with a sufficiently small error.

§3. Results

In order to test the feasibility of our SA inversion method, we compute sets of ECT synthetic data for four typical permittivity distributions by solving the forward problem. We simulate a twelve-electrode ECT sensor and compute the capacitance values for all single-electrode combinations. We consider two-component distributions with a lower permittivity material of 1.0 (air) and a higher permittivity material of 2.5 (oil). We restrict our numerical test to the reconstruction of noise free ECT data in three first cases and we include noisy data for the fourth case. SA algorithm is implemented in Fortran 90 on a Pentium IV personal computer with a 1.7 MHz CPU and 512 Mbytes memory. We experimented with a 120 by 60 grid to reduce inversion times but results are valid for any larger dimensions.

After an appropriate parametrization, SA produces satisfactory results for all four study cases. In figure 4, we present image reconstructions for a simplified annular flow, a stratified and a bubble flow after 30,000 and 60,000 forward problem computations. Our application of SA to the inversion of synthetic ECT data provides us very encouraging results. One criticism of SA is its relatively high computation time. An interesting possibility which we are now exploring is the use of high performance parallel computation and spline regularization techniques.

In the fourth case (four gas bubbles in an oil matrix), the sensor geometrical configuration is close to the one of our laboratory sensor and the permittivity distribution is a bubbly flow. We compute the 132 synthetic capacitances C_{ij} for the 12 problems. These data are perturbed with a 10% random noise function. The true calculated data and the data with noise are inverted using the permittivity arrangement process described in the previous section. The images are

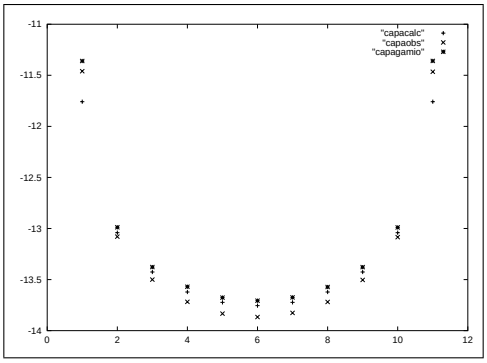

Figure 1: Experimental (cross) and Computed capacitances using FVM(+) and FEM(*) methods

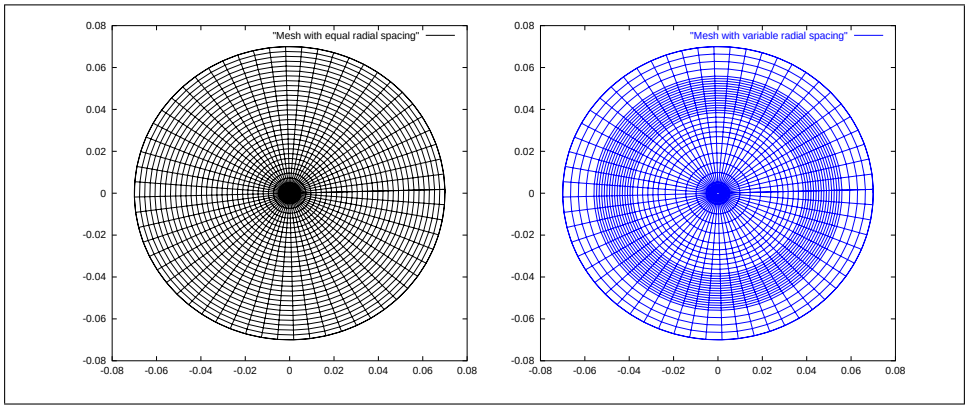

Figure 2: Regular(left) and Variable (right) grid meshes

very close one from the other as can be seen in last snapshot of figure 5. The algorithm seems to converge towards an equivalent permittivity distribution and is a good candidate for image reconstruction with random noise.

The process has been stopped at 60,000 forward problem calculations for all cases in order to compare the image reconstruction achievements.The L^2 norm for the objective misfit function between data and computed capacitances has been chosen. The computational costs are approximately the same around 25 minutes. Convergence is relatively fast in the first 10,000 iterations, then crosses a slow phase till 30,000 steps and accelerates until the process ends.

§4. Conclusions

The application of SA to the inversion of measured ECT data has provided us encouraging results. One significant disadvantage of SA relative to linear methods is its high computational time as several thousands of forward problem computations are required. This method does not require a good initial model and is successful to invert synthetic data with noise and without noise. In order to have good results in inverting real data, an acceleration procedure will be explored by using a spline regularization in space which can allow a reduction of the number of parameters by an order of magnitude.

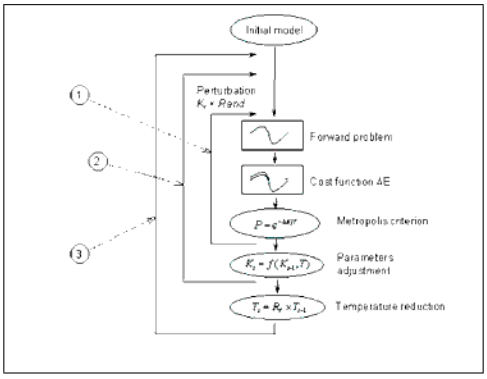

Figure 3: Schematic explanation of the Simulated Annealing algorithm

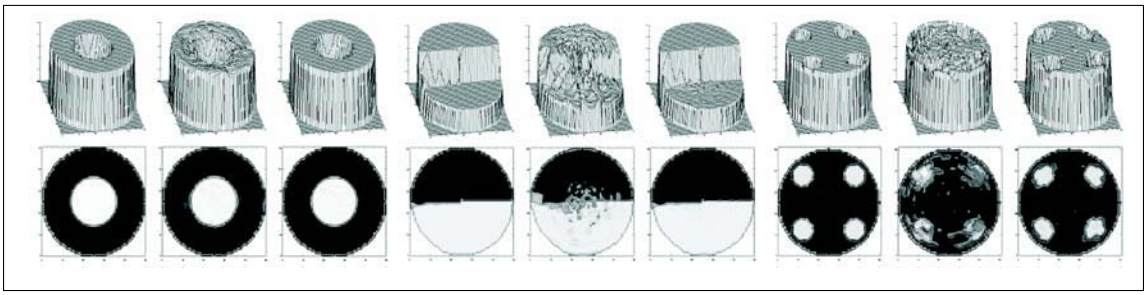

Figure 4: Reconstructed images at 30000 and 60000 iterations for annular (left), stratified(middle) and bubbly flows(right). The reference models are the first images of each series of three snapshots.

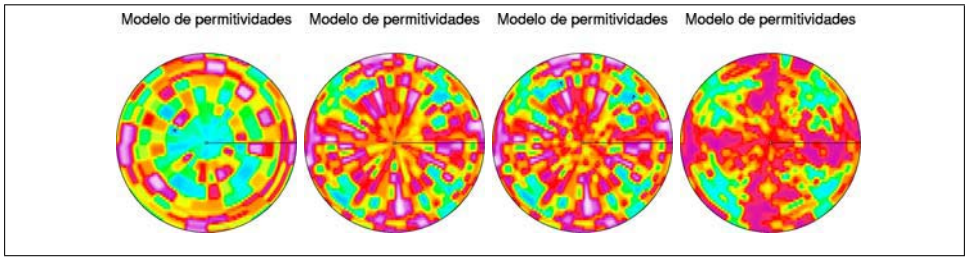

Figure 5: Reconstructed images at 10, 20, 30, 50 and 60000 iterations for bubbly flows in the case of a reallistic sensor configuration and data with noise

Acknowledgements

We thank W.Q. Yang for his fruitful discussions on inversion algorithms applied to capacitance tomography. This contribution was supported by projects IMP/D.00117 and IMP/D.00046.

References

[1] BECK M.S., BYARS M., DYAKOWSKI T., WATERFALL R., HE R., WANG S.M. AND YANG W.Q. Principles and industrial applications of electrical capacitance tomography. *Measurement+Control 30*, 1997, pp. 197–200.

[2] GALLAGHER K., SAMBRIDGE M. AND DRIJKONINGEN G. Genetic algorithms: an evolution from Monte Carlo Methods for strongly non-linear geophysical optimization problems. *Geophys. Res. Lett. 18*, 1991, pp. 2177–2180.

[3] HUANG S.M., XIE C.G., VASINA J, LENN C., ZHANG B.F. AND BECK M.S. Experimental evaluation of capacitance tomographic flow imaging system using physical models. In *1st ECAPT Conf. European Concerted Action on Process Tomography*, Manchester, 1992, pp 347–360.

[4] ISAKSEN O. AND NORDTVEDT J.E. A new reconstruction algorithm for process tomography. *Meas. Sci. Tech. 4*, 1993, pp. 1464–1475.

[5] METROPOLIS N., ROSENBLUETH A., ROSENBLUETH M., TELLER A. AND TELLER E. Equation of state calculations by fast computing machines. *J. Chem. Phys. 21*, 1953, pp. 1087–1092.

[6] C. ORTIZ-ALEMAN, R. MARTIN AND J. C. GAMIO Application of simulated annealing and genetic algorithms to the reconstruction of electrical permittivity images in capacitance tomography. In *3rd World Congress on Industrial Process Tomography*, Banff, Canada, 2003, (CD Conference Proceedings)

[7] PLASKOWSKI A.B., BECK M.S., THORN R. AND DYAKOWSKI T. *Imaging Industrial Flows.* Applications of Electrical Process Tomography, Bristol, IOP, 1995.

[8] VASUDEVAN K., WILSON W. G. AND LADILAW W. Simulated annealing static computation using an order-based energy function. *Geophysics 56*, 1991, pp. 1831–1839.

[9] XIE C.G., PLASKOWSKI A. AND BECK M.S. 8-electrode capacitance system for two-component flow identification. Part 1: Tomographic flow imaging. *IEE Proceedings A 136 (4)*, 1989, pp. 173–183.

[10] XIE C.G., HUANG S.M., HOYLE B.S., THORN R., LENN C. AND BECK M.S.Electrical capacitance tomography for flow imaging - system model for development of reconstruction algorithms and design of primary sensors. *IEE Proc. G 139*, 1992, pp. 89-98.

[11] YANG W.Q. AND PENG L. Image reconstruction algorithms for electrical capacitance tomography. *Meas. Sci. Tech. 14*, 2003, pp. 1-13.

Roland Martin, Carlos Ortiz-Aleman and Carlos Gamio
Mexican Petroleum Institute
152 Eje Lazaro Cardenas 07730 Mexico City
rmartin@imp.mx and jcortiz@imp.mx